Int. J. Nano Dimens., 11 (2): 168-176, Spring 2020

ORIGINAL ARTICLE

Detecting compressive strain by evaluation of Raman spectroscopy of the multiwall Carbon nanotubes/TiO_2 nanocomposites

Marzieh Nadafan[1,*], Ammar Shaker Alattar[2], Zahra Dehghani[3], Rasoul Malekfar[4]

[1] Department of Physics, Shahid Rajaee Teacher Training University, Tehran, Lavizan, Iran
[2] Department of Physics, University of Mustansiriyah, Baghdad, IQ, Iraq
[3] Department of Physics, University of Neyshabur, Neyshabur, Iran
[4] Atomic and Molecular Physics Group, Faculty of Basic Sciences, Tarbiat Modares University, Tehran, Iran

Received 17 February 2020; revised 13 March 2020; accepted 25 March 2020; available online 10 April 2020

Abstract

Functionalized Multi-walled carbon nanotubes (*f*-MWCNTs) which are modified using nitric acid and sulfuric acid were evaluated to synthesize a uniform nanocomposite via application of TiO_2. The *f*-MWCNTs-TiO_2 nanocomposites have been produced via using the chemical simple two-step method. To characterize the structural analysis, scanning electron microscopy (SEM) imaging, ultraviolet-visible (UV-Vis) spectroscopy, and Raman spectroscopy were utilized. The maximum shift of D, G, and 2G-bands of *f*-MWCNTs were related to 20 wt. % *f*-MWCNTs in TiO_2 nanoparticles. Moreover, an up-shift of 40 cm^{-1} was recorded for the MWCNTs (G'-band) for 5 wt. % *f*-MWCNTs. For 20 wt. % *f*-MWCNTs/TiO_2 (G-band) nanocomposites, ε_z was determined by 4.7%. By increasing the amount of f-MWCNTs in *f*-MWCNs/TiO_2 nanocomposite, the compressive strain was increased. Among the four bonds, the G'-band behaved differently against increasing *f*-MWCNTs. The shifting frequency of G-band indicates the strong interaction between *f*-MWCNTs and TiO_2 nanoparticles. The interaction between *f*-MWCNTs and TiO_2 nanoparticles, identified by the Gruneisen parameter. Therefore, a mechanism generated for stress transfer at the interface between *f*-MWCNTs and TiO_2 nanoparticles which is indicated in many significant increases obtained in the mechanical and acoustical properties.

Keywords: *Compressive Strain; Multiwalled Carbon Nanotubes; Nanocomposites; Raman Spectroscopy; Titanium Dioxide.*

How to cite this article

Nadafan M, Shaker Alattar M, Dehghani Z, Malekfar R. Detecting compressive strain by evaluation of Raman spectroscopy of the multiwall Carbon nanotubes/TiO_2 nanocomposites. Int. J. Nano Dimens., 2020; 11 (2): 168-176.

INTRODUCTION

Recently, carbon nanomaterials have attracted considerable attention in the field of material science. Individual Carbon nanotubes (CNTs) are used for a wide range of unique properties for instance electrical conductance, thermal resistance, high chemical stability, and making exciting materials to a broad range of industries [1]. In the last decade, many scientific efforts were undertaken for the fabrication of multifunctional metal nanoparticle-CNT nanohybrids that take advantage of the unique combination of mechanical, electrical, and thermal properties from each of them [2]. There are many reports on the fabrication of noble metals (such as Pt, Pd, Ru, Ag, and Au) or nanoparticle-decorated CNTs as well as evaluation of their electrical, magnetic, and optical aspects [3]. On the other hand, some materials containing Titania (TiO_2) are used widely to remove different chemical pollutants from water or air. Also, the photocatalytic activity of TiO_2 for solving environmental problems is remarkable [4]. Composite materials containing CNTs and TiO_2 have the large surface area, high adsorption capacity as well as removing a high range of pollutants. They have attracted more consideration rather than other materials [5, 6].

* Corresponding Author Email: *m.nadafan@sru.ac.ir*

As the curiosity and interest of characterizing carbon nanomaterials surged, the demand for processing, modification, and customization of these materials increased. Raman spectroscopy is a powerful and non-destructive technique that is quite suitable for detecting a different kinds of characterizations needed with most of all materials. It evaluates the associated vibrational features (band frequencies and widths) [7]. Raman spectroscopy can also detect the diameter of CNTs [8], the disorder in the carbon systems [9], and the effect of nanotube-nanotube interactions [10] on the vibrational modes.

Furthermore, Raman spectroscopy is used for evaluating the compressive strain of CNTs nanocomposites. The strain is a crucial important in device performance or to improve mobility, which is used in modern microelectronics. It changes the crystal phonons with tensile strain resulting in mode softening, and the opposite for compressive or uniaxial strain [7]. The magnitude of the shift of phonon frequencies with strain is proportional to the Gruneisen parameter, so by monitoring phonons and considering the phonon's frequency; the Gruneisen parameter is detected [7]. Although the Gruneisen parameter is a critical key in applied subjects, it is less pointed out by researchers right now.

In this research, we synthesized functionalized Multiwalled carbon nanotubes (*f*-MWCNTs)-TiO_2 nanocomposite in a two steps process: synthesis of TiO_2 nanocomposite by sol-gel method and then followed by the decoration of TiO_2 nanocomposites over the *f*-MWCNTs. Scanning electron microscopy (SEM) imaging, ultraviolet-visible (UV-Vis), and Raman spectroscopy of the above nanocomposite were done. The roles of *f*-MWCNTs concentration in the Gruneisen parameter and compressive strain of *f*-MWCNTs nanocomposites have been discussed in detail.

EXPERIMENTAL PROCEDURE

Acid treatment of MWCNTs

The chemical vapor deposition (CVD) MWCNTs with a mean length of about micrometer was supplied. Different research groups reported that modification of CNTs surface could improve dispersion and transfer of stress in the host nanoparticles [11-13]. Therefore, in order to ameliorate the functionality of MWCNTs, the mixture acid, nitric acid (60%) and sulfuric acid (95-97%) with 1:3 ratio was chosen. The MWCNTs was added to the previous solution for 100 min under 100 ºC heater-stirrer. After this, the *f*-MWCNTs was set in the oven under 70 ºC for 30 min. This procedure is required to preparation of nanotubes to continue research path.

Preparation of f-MWCNTs/TiO_2

The synthesis procedure of *f*-MWCNTs/TiO_2 nanocomposites consists of adding 8.5 ml of Titanium propoxide (TBOT, 98%) to 25 ml of ethanol (≥ 99%) used as the solvent. The mixture was kept under vigorous magnetic stirring for 10 min at room temperature. After that, 2.0 ml of nitric acid was added and the stirring performed for 60 min. The different amount of *f*-MWCNTs was added to the last solution and stirred for one day until a dry gel was taken. For preparing the anatase phase of TiO_2, it is necessary to put this gel into the oven till 450 ºC. These nanocomposites are ready for later analysis.

Characterization

The morphology and microstructure of the synthesized samples were investigated by SEM Seron Technology-AIS2100 model after coating the samples with a thin layer of gold. The linear absorption spectra for all the samples were obtained using a UV-VIS spectrophotometer (PG Instrument UV-Visible system, model T80+). Raman spectra were acquired by a Raman spectrometer using a 1064 nm Nd : YLF laser excitation source. Raman spectroscopy was utilized for the estimation of the magnitude of strain by observing the shifts of the whole bands of nanocomposites.

RESULT AND DISCUSSION

SEM analysis

The SEM was used to assess the morphology of the pure MWCNTs and *f*-MWCNTs/TiO_2 nanocomposites. The SEM images of nanocomposites are shown in Fig. 1. The uniform distribution of TiO_2 over the *f*-MWCNTs surface is observable. The diameter of the MWCNTs was 32–40 nm where the thickness of the TiO_2 nanoparticles was estimated to be in the 30–45 nm range. Lengths of purified MWCNTs were not appreciably changed after acid functionalization of them.

Analyzing UV-Vis spectra

Fig. 2 depicts the UV-Vis spectra of *f*-MWCNTs/TiO_2, TiO_2, *f*-MWCNTs and pristine MWCNTs. The

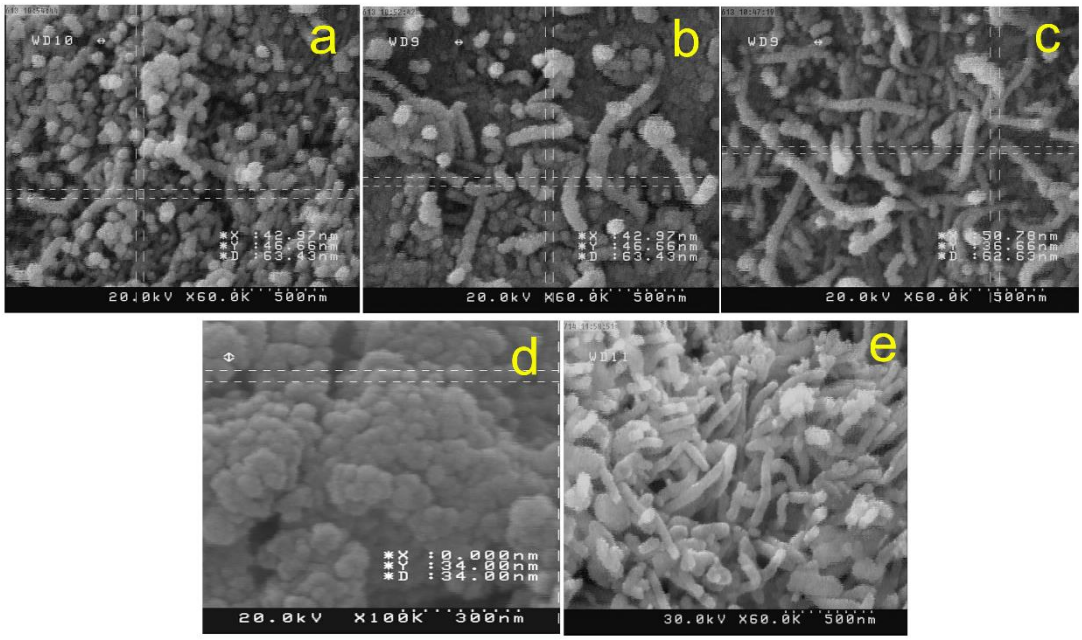

Fig. 1. Scanning electron microscopy imaging of (a) 5% MWCNTs/TiO_2 (b) 10% MWCNTs/TiO_2 (c) 20% MWCNTs/TiO_2 (d) TiO_2 nanoparticles and (e) MWCNTs.

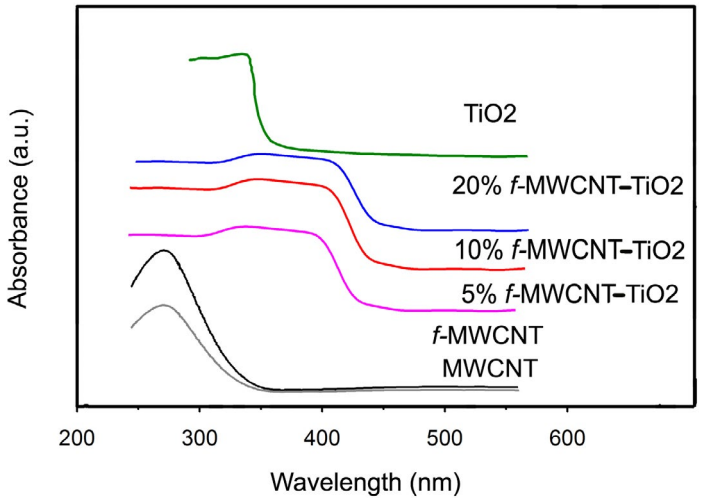

Fig. 2. Ultraviolet-Visible absorption spectra of MWCNTs, functionalized MWCNTs, 5% MWCNTs/TiO_2, 10% MWCNTs/TiO_2, 20% MWCNTs/TiO_2 and TiO_2 nanoparticles.

strong peak around 275 nm shows that MWCNTs were successfully dispersed in ethanol solution. The absorption peak intensity is increased due to the *f*-MWCNTs suspension was dispersed more successfully in comparison with pristine MWCNTs in the same solution. The polar functional group on the surface of MWCNTs may be increased the dispersion of them in the solution. The effect of the modified sidewall in the dispersing of MWCNTs well compromised with other researches [14, 15]. About other spectra, spectral shapes are the same in most regions, but there are partially different in the absorption edges. The absorption edges of *f*-MWCNTs/TiO_2 nanocomposites are extended toward the visible region, so it started at about 430 nm. For pure TiO_2 nanoparticles, it is about

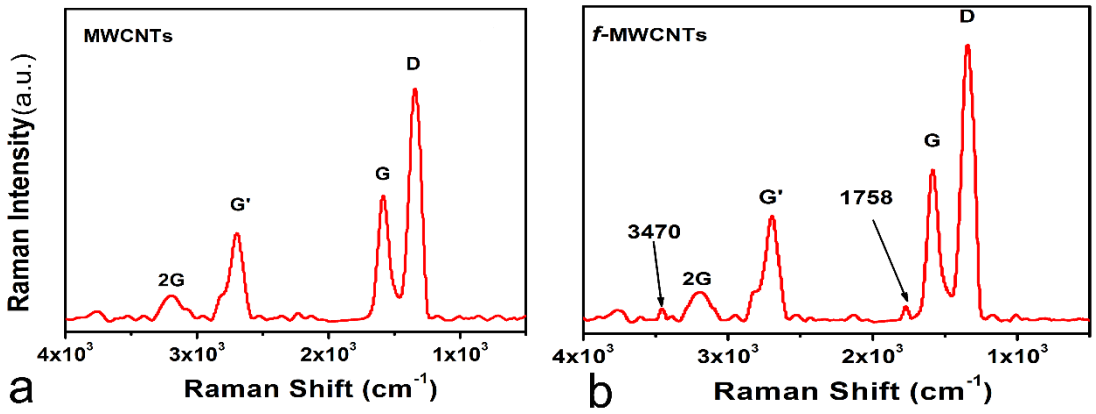

Fig. 3. Raman spectra of (a) MWCNTs (b) *f*-MWCNTs.

380 nm. The existence of TiO_2 nanoparticles and the strong contact with *f*-MWCNTs are the main point of the red shifting of *f*-MWCNTs/TiO_2 UV-Vis spectra. It may be for generating a new band gap that causes a red shift in UV-Vis spectra.

The direct band gap energy for the 0% *f*-MWCNTs/TiO_2, 5% *f*-MWCNTs/TiO_2, 10% *f*-MWCNTs/TiO_2, and 20% *f*-MWCNTs/TiO_2 samples calculated. In the case of the above samples, the absorption edges shifted to red light, and their bandgaps were 2.83, 2.40, 2.34, and 2.30 eV, respectively. The results show that by the introduction of MWCNTs the visible light absorption of the TiO_2 samples is improved, and the doped samples can be excited by visible light.

Raman spectroscopy analysis

Raman spectra of pure MWCNTs

Fig. 3(a) was presented Raman peaks of pristine MWCNTs. Accordingly, four main peaks was seen called D, G′, G and D′ or 2G. The two main typical graphite bands are present in the Raman spectrum of MWCNTs bundles: the band at 1583 cm^{-1} (G band) assigned to the in-plane vibration of the C–C bond and the band at 1345 cm^{-1} (D band) activated by the presence of the defects and structural disorder in CNTs [16].

The Raman spectrum (Fig. 3 (a)) also exhibits the 2G band is around 3179 cm^{-1}, and a band at 2672 cm^{-1} called the G' band which attributed to the overtone of the D band. These bands have been obtained in the as-received powder of bundled MWCNTs.

The D and G bands can be used for characterizing materials or detecting structural modifications of the nanotube sidewalls that originate from the existence of the defects and adding some chemical species. The upshifts/downshifts in Raman modes especially in the G band is because of charge transferring related to acceptor/donor features [17, 18].

There is four applications of G band frequency for MWCNTs that are characterized diameter of MWCNTs, metallic or semiconductor phase distinction, detection of the charge transfer from dopant and estimating the results of different selection rules in Raman spectra. The increasing or decreasing intensity inline shape of metallic or semiconducting phase is related to charge transfer of dopant to MWCNTs [18, 19].

Fig. 3 (b) was shown the Raman spectra of *f*-MWCNTs. Also, the four above bands are in the Raman spectrum of *f*-MWCNTs. Furthermore, there are two bands at 1758 cm^{-1} and 3470 cm^{-1} that are related to the characteristic of C=O and O–H stretching modes in carboxylic acid groups, respectively [20]. The results reveal that carboxylic acid groups have been attached to the surface of MWCNTs, as well.

Raman spectra of f-MWCNTs/TiO_2

Raman spectra of TiO_2 and *f*-MWCNTs/TiO_2 were shown in Figs. 4, 5, and 6. The Raman spectrum of TiO_2 shows peaks located at 387, 513 and 633 cm^{-1} due to the lattice vibrational mode of the anatase TiO_2 [21]. As shown in Fig. 5, the Raman intensity of the main peaks of *f*-MWCNTs was measured versus excitation energy (eV). However, there is no difference between graphs in Fig. 5 and Fig. 6. As shown in Fig. 6, the G′-band

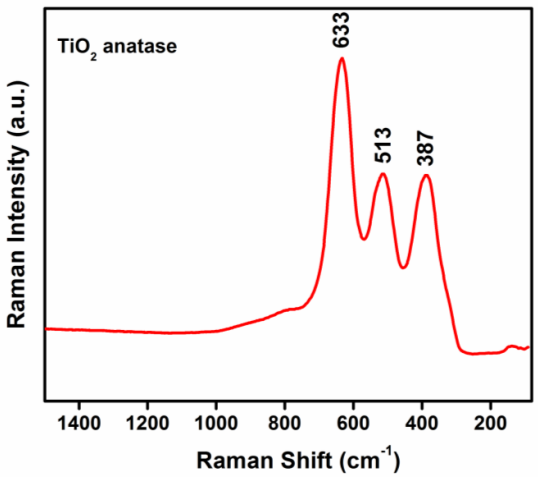

Fig. 4. Raman spectrum of TiO_2 nanoparticles.

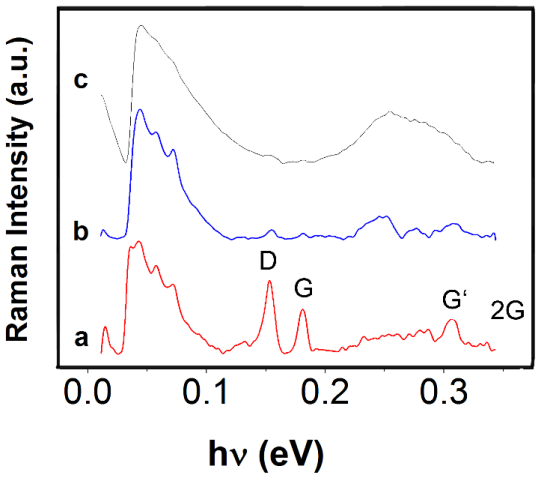

Fig. 5. Raman spectra of *f*-MWCNTs/TiO_2 by loading (a) 5%, (b) 10% and (c) 20% *f*- MWCNTs versus excitation energy.

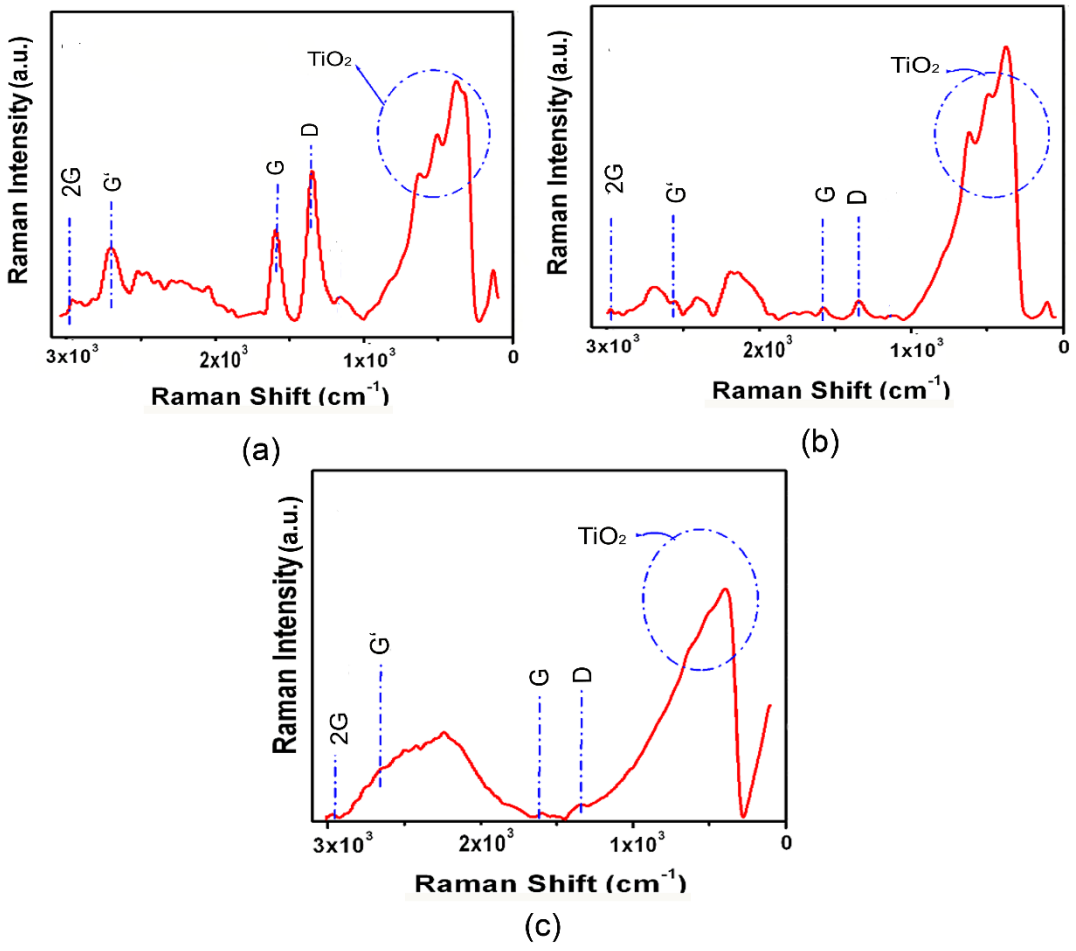

Fig. 6. Raman spectra of *f*-MWCNTs/TiO_2 by loading (a) 5%, (b) 10% and (c) 20% *f*-MWCNTs.

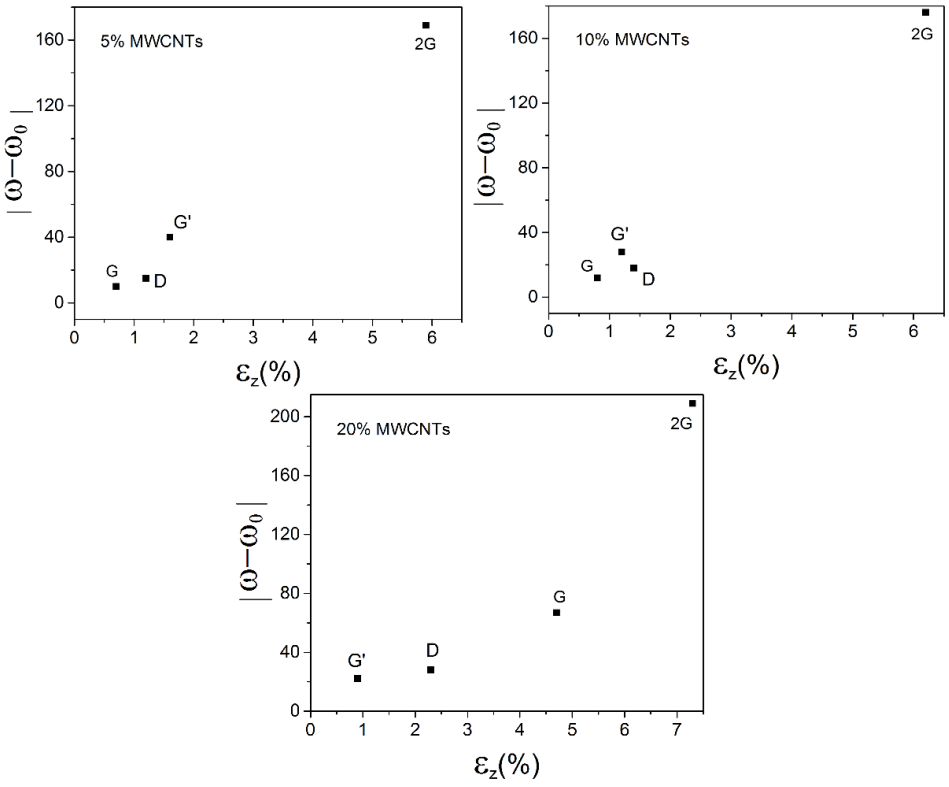

Fig. 7. Raman band shift of *f*-MWCNTs/TiO_2 versus the compressive strain (%).

of *f*-MWCNTs/TiO_2 is approximately at the same position. The presence of D, 2G, and G-bands in *f*-MWCNTs/TiO_2 nanocomposites confirms the interfacial interaction between *f*-MWCNT and TiO_2 [21]. By loading *f*-MMWCNTs up to 20 wt. %, all the bands associated to TiO_2 in *f*-MWCNTs/TiO_2 was decreased in intensity. For instance, increasing the intensity of the D band indicates that the extent of sp^2 hybridized carbon was more aligned. According to the 1582 cm^{-1} band as well as 2645 cm^{-1} one; an overtone mode of the D band, incorporation of TiO_2 nanoparticles is the least affected on MWCNTs. The main three bands of anatase TiO_2 in the Raman spectrum are narrowed by loading MWCNTs up to 20 wt.%. Moreover, the Raman band at 1332 cm^{-1} is more broadening in *f*-MWCNTs/TiO_2 than pristine MWCNTs may be due to the strain gradients originating from interface integration of TiO_2 and MWCNTs [1].

In Raman spectra, the relative shift depends on the direction of the *f*-MWCNTs axis and is maximal in the direction of the applied stress. Because the *f*-MWCNTs in the composites may have arbitrary direction, it was evaluated an average shift of all band peaks [22]. The proposed mechanism of this composite is that the MWCNTs tent to absorb the electron cloud; then by increasing of MWCNTs, the electronic absorption will be increase. This can tend to less flux of electron and electrical conductivity in the system. These results cause an electron is more stable and more sedentary. It is possible for the Raman data to estimate the compressive strain of CNTs because of using Eq. (1):

$$\Delta\omega^{\pm}/\omega_0 = -\gamma(1-\nu)\varepsilon_z \quad (1)$$

Where $\Delta\omega^{\pm}/\omega_0$ is the relative shift of the (D, G, G', and 2G)-band cm^{-1}, γ is known as the Gruneisen parameter which describes the frequency shift under hydrostatic strain and can be approximated to 1.24 for CNTs, υ is the Poisson ratio and taken to be 0.28 and υ is the compressive strain [23]. According to Figs. 7 and 8, the maximum shift of D, G, and 2G-bands of *f*-MWCNTs were related to 20 wt. % *f*-MWCNTs in TiO_2 nanoparticles. Moreover, an up-shift of 40 cm-1 was recorded for the MWCNTs (G'-band) for 5 wt. % *f*-MWCNTs. For 20

Table 1. The compressive strain of the main bands of f-MWCNTs in TiO_2 nanoparticles matrix.

Sample	band	Blank MWCNT	ω_{band}	$\varepsilon_z(\%)$	$\varepsilon_{z,\max}(\%)$
5 wt.% MWCNT	D	1363 cm^{-1}	1348 cm^{-1}	1.2	---
	G	1583 cm^{-1}	1593 cm^{-1}	0.7	---
	G'	2672 cm^{-1}	2712 cm^{-1}	1.6	1.6
	2G	3179 cm^{-1}	3010 cm^{-1}	5.9	---
10 wt.% MWCNT	D	1363 cm^{-1}	1345 cm^{-1}	1.4	---
	G	1583 cm^{-1}	1595 cm^{-1}	0.8	---
	G'	2672 cm^{-1}	2700 cm^{-1}	1.1	---
	2G	3179 cm^{-1}	3003 cm^{-1}	6.2	---
20 wt.% MWCNT	D	1363 cm^{-1}	1335 cm^{-1}	2.3	2.3
	G	1583 cm^{-1}	1650 cm^{-1}	4.7	4.7
	G'	2672 cm^{-1}	2650 cm^{-1}	0.9	---
	2G	3179 cm^{-1}	2970 cm^{-1}	7.3	7.3

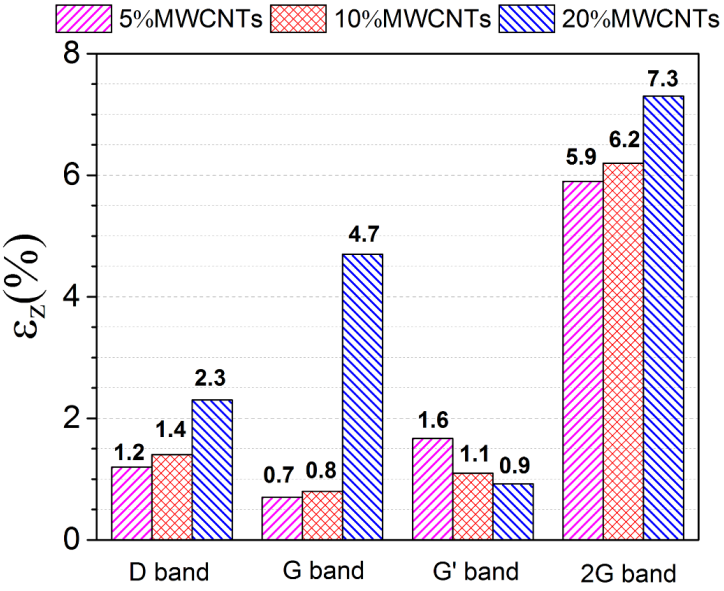

Fig. 8. The compressive strain of the main bands of *f*-MWCNTs in TiO_2 nanoparticles.

wt. % *f*-MWCNTs/TiO2 (G-band) nanocomposites, ε_z was determined 4.7%, almost three and twenty four time greater than that reported for PU/MWCNT and an epoxy/SWCNT composite [24]. The shifting frequency of G-band indicates the strong interaction between *f*-MWCNTs and TiO_2 nanoparticles. So, it begets the mechanism for stress transfer at the interface between *f*-MWCNTs and TiO_2 nanoparticles that is pointed out in the large increases in the mechanical and acoustical properties obtained [24-27]. We made an effort to achieve a measurement of compressive strain of all samples in four main bands of MWCNTs. These results are tabulated in Table. 1.

By increasing the amount of f-MWCNTs in f-MWCNs/TiO2 nanocomposite, the compressive strain was increased (Fig. 8). Among the four bonds, the G'-band behaved differently against increasing *f*-MWCNTs. The significant down (up)-shifting of G′-band can demonstrate the axial elongation (shortening) of the C-C bond length in nanotube shell [22, 28]. Following literature data, if the corresponding ε_z is behavior 1, the strain behavior should be still that of elastic response [25-27]. This response was given in some percentages of *f*-MWCNTs as loading of 10 wt. %

and 20 wt.% *f*-MWCNTs.

It is proved the annealing process can be removed from the upshift of G band frequency but the thermal treatment confirms the upshifts of G band. In some researches, the detection of the intrinsic frequencies of D and G bands is an issue important for analyzing the Raman spectra of samples [29].

The two factors, doping (n) and strain (ε) can change and shift the Raman mode frequencies of the G and G' modes. These changes were assessed by applying the correlation analysis proposed [29, 30]. On the other hand, in low charge carrier concentrations, the shift of G' band as a function of n is negligible, compared to the change in G mode [30].

CONCLUSION

In this work, the *f*-MWCNTs/TiO_2 nanocomposite was made by the simple chemical method at the loading fractions from 0 wt.% to 20 wt.% *f*-MWCNTs. Firstly, the synthesis of TiO_2 nanoparticles by sol-gel method and then followed by the decoration of TiO_2 nanoparticles over the *f*-MWCNTs. Results of SEM illustrated imaging, the uniform distribution of TiO_2 over the *f*-MWCNTs surface is observable. The diameter of the *f*-MWCNTs was 32–40 nm where the thickness of the TiO_2 nanoparticles was estimated to be in the 30–45 nm range. In UV-Vis absorption spectra, the absorption edges of *f*-MWCNTs/TiO_2 nanocomposites extended toward the visible region and started at about 430 nm. For pure TiO_2 nanoparticles, it is about 380 nm. The existence of TiO_2 nanoparticles and the strong contact with *f*-MWCNTs are the main points of the red shifting of *f*-MWCNTs/TiO_2 in UV-Vis spectra.

We show that the Raman spectroscopy can be successfully utilized for the estimation of the magnitude of strain by observing the shifts of *f*-MWCNTs bands. Then, the roles of *f*-MWCNTs concentration in the Gruneisen parameter and compressive strain of *f*-MWCNTs nanocomposites have been discussed by Raman spectroscopy. The maximum shift of D, G, and 2G-bands of *f*-MWCNTs were related to 20 wt. % *f*-MWCNTs in TiO_2 nanoparticles. Moreover, an up-shift of 40 cm-1 was recorded for the MWCNTs (G'-band) for 5 wt. % *f*-MWCNTs. For 20 wt. % *f*-MWCNTs/TiO2 (G-band) nanocomposites, ε_z was determined 4.7%. By increasing the amount of *f*-MWCNTs in *f*-MWCNs/TiO2 nanocomposite, the compressive strain was increased. Among the four bonds, the G'-band behaved differently against increasing *f*-MWCNTs. The results confirm the ability of Raman spectroscopy to monitor the dispersion and the loading of *f*-MWCNTs in *f*-MWCNTs/TiO_2 nanocomposites. Then, it provides the mechanism for stress transfer at the interface between *f*-MWCNTs and TiO_2 nanoparticles that is pointed in the large increases in the mechanical and acoustical properties obtained. These results did not have mentioned in other research papers so far. Furthermore, it can be concluded that the synthesized samples are promising candidates for future acoustical and mechanical applications.

ACKNOWLEDGEMENT

This work was supported by Shahid Rajaee Teacher Training University under contract number 15559.

CONFLICT OF INTEREST

The authors declare that they have no competing interests.

REFERENCES

[1] Alijani H., Tayyebi S., Hajjar Z., Shariatinia Z., Soltanali S., (2017), Prediction of the Carbon nanotube quality using adaptive neuro–fuzzy inference system, *Int. J. Nano Dimens.* 8: 298-306.

[2] Beitollahi H., Safaei M., Tajik S., (2019), Application of Graphene and Graphene Oxide for modification of electrochemical sensors and biosensors: A review. *Int. J. Nano Dimens.* 10: 125-140.

[3] Zhang F. J., Chen M. L., Oh W. C., (2010), Photoelectrocatalytic properties of Ag-CNT/TiO_2 composite electrodes for methylene blue degradation. *New Carbon Mater.* 25: 348–356.

[4] Muruganandham M., Shobana N., Swaminathan M., (2006), Optimization of solar photocatalytic degradation conditions of Reactive Yellow 14 azo dye in aqueous TiO_2. *J. Mol. Catal. A Chem.* 246: 154-161.

[5] Kochana J., Adamski J., (2012), Detection of NADH and ethanol at a graphite electrode modified with titania sol-gel/Meldola's Blue/MWCNT/Nafion nanocomposite film. *Cent. Eur. J. Chem.* 10: 224-231.

[6] Larijani M. M., Safa S., (2014), Increase of hydrogen storage capacity of CNTs by using transition metal, metal oxide-CNT nanocomposites. *Acta Phys. Pol. A*. 126: 732-735.

[7] Mohiuddin T. M. G., Lombardo A., Nair R. R., Bonetti A., Savini G., Jalil R., Bonini N., Basko D. M., Galiotis C., Marzari N., Novoselov K. S., Geim A. K., Ferrari A. C., (2009), Uniaxial strain in graphene by Raman spectroscopy: G peak splitting, Gruneisen parameters, and sample orientation. *Phys. Rev. B: Condens. Matter*. 79: 205433.

[8] Graupner R., (2007), Raman spectroscopy of covalently functionalized single-wall carbon nanotubes. *J. Raman Spectrosc.* 38: 673–683.

[9] Cuesta A., Dhamelincourt P., Laureyns J., Martinez-Alonso A., Tascon J. M. D., (1994), Raman microprobe studies on carbon materials. *Carbon.* 32: 1523–1532.

[10] Rao A. M., Chen J., Richter E., Schlecht U., Eklund P. C., Haddon R. C., Venkateswaran U. D., Kwon Y. K., Tomanek D., (2001), Effect of van der Waals Interactions on the Raman modes in single walled Carbon nanotubes. *Phys. Rev. Lett.* 86: 3895–3898.

[11] .Bandarian M., Shojaei A., Rashidi A. M., (2011), Thermal, mechanical and acoustic damping properties of flexible open-cell polyurethane/multi-walled carbon nanotube foams: Effect of surface functionality of nanotubes. *Polym. Int.* 60: 475-482.

[12] Roy D., Bhattacharyya S., Rachamim A., Plati A., Saboungi M. L., (2010), Measurement of interfacial shear strength in single wall carbon nanotubes reinforced composite using Raman spectroscopy. *J. Appl. Phys.* 170: 043501.

[13] Ajayan P. M., Suhr J., Koratkar N., (2006), Utilizing interfaces in carbon nanotube reinforced polymer composites for structural damping. *J. Mater. Sci.* 41: 7824-7829.

[14] Rausch J., Zhuang R. C., Mader E., (2010), Surfactant assisted dispersion of functionalized multi-walled carbon nanotubes in aqueous media. *Comp. Part A*. 41: 1038-1046.

[15] Tang Q. Y., Shafiq I., Chan Y. C., Wong N. B., Cheung R., (2010), Study of the dispersion and electrical properties of Carbon nanotubes treated by surfactants in Dimethylacetamide. *J. Nanosci. Nanotechnol.* 10: 4967-4974.

[16] Zhang H. B., Lin G. D., Zhou Z. H., Dong X., Chen T., (2002), Raman spectra of MWCNTs and MWCNT-based H_2 adsorbing system. *Carbon.* 40: 2429-2436.

[17] Corio P., Santos P. S., Brar V. W., Samsonidze Ge. G., Chou S. G., Dresselhaus M. S., (2003), Potential dependent surface Raman spectroscopy of single wall carbon nanotube films on platinum electrodes. *Chem. Phys. Lett.* 370: 675-682.

[18] Souza Filho A. G., Jorio A., Samsonidze Ge. G., Dresselhaus G., Saito R., Dresselhaus M. S., (2003), Raman spectroscopy for probing chemically/physically induced phenomena in carbon nanotubes. *Nanotechnol.* 14: 1130-1139.

[19] Dresselhaus M. S., Dresselhaus G., Saito R., Jorio A., (2005), Raman spectroscopy of carbon nanotubes. *Phys. Rep.* 409: 47-99.

[20] Hadavand B. S., Mahdavi Javid K., Gharagozlou M., (2013), Mechanical properties of multi-walled carbon nanotube/epoxy polysulfide nanocomposite. *Mater. Des.* 50: 62–67.

[21] Chaudhary D., Singh S., Vankar V. D., Khare N., (2017), A ternary Ag/TiO_2/CNT photoanode for efficient photo electrochemical water splitting under visible light irradiation. *Int. J. Hydrog. Energy.* 42: 7826-7835.

[22] Laurenzi S., Botti S., Rufoloni A., Santonicola M. G., (2014), International symposium on dynamic response and failure of composite materials, DRaF2014 fracture mechanisms in epoxy composites reinforced with carbon nanotubes. *Procedia Eng.* 88: 157-164.

[23] Hadjiev V. G., Warren G. L., Sun L., Davis D. C., Lagoudas D. C., Sue H. J., (2010), Raman microscopy of residual strains in carbon nanotube/epoxy composites. *Carbon.* 48: 1750-1756.

[24] McCloy C., McNally T., Brennan G. P., Erskine J., (2007), Thermosetting polyurethane multiwall carbon nanotube composites. *J. Appl. Polym. Sci.* 105: 1003-1011.

[25] Saito R., Dresselhaus G., Dresselhaus M. S., (1993), Electronic structure of double layer graphene tubules. *J. Appl. Phys.* 73: 494-500.

[26] Cooper C. A., Young R. J., Halsall M., (2001), Investigation into the deformation of carbon nanotubes and their composites through the use of Raman spectroscopy. *Composites Part A*. 32: 401-411.

[27] Rao A. M., Richter E., Bandow S., Chase B., Eklund P. C., Williams K. A., Fang S., Subbaswamy K. R., Menon M., Thess A., Smalley R. E., Dresselhaus G., Dresselhaus M. S., (1997), Diameter-selective Raman scattering from vibrational modes in Carbon nanotubes. *Science.* 275: 187-191.

[28] Grimmer C. S., Dharan C. K. H., (2010), Enhancement of delamination fatigue resistance in carbon nanotube reinforced glass fiber/polymer composites. *Compos. Sci. Technol.* 70: 901-908.

[29] Lee J. E., Ahn G., Shim J., Lee Y. S., Ryu S., (2012), Optical separation of mechanical strain from charge doping in graphene. *Nat. Commun.* 3: 1024-1029.

[30] Vejpravova J., Pacakova B., Endres J., Mantlikova A., Verhagen T., Vales V., Frank O., Kalbac M., (2015), Graphene wrinkling induced by monodisperse nanoparticles: Facile control and quantification. *Sci. Rep.* 5: 15061-15067.